Electron Redistribution in $Pt_2(dta)_4I$: From Building Blocks to the Infinite Chain. A Theoretical Investigation of Possible Peierls Distortions

Vincent Robert,[†,‡] Sébastien Petit,[†] and Serguei A. Borshch*[,†]

Institut de Recherches sur la Catalyse, UPR 5401 CNRS, 2, avenue Albert Einstein, 69626 Villeurbanne Cedex, France, Laboratoire de Chimie Théorique, Ecole Normale Supérieure de Lyon, 46, allée d'Italie, 69364 Lyon Cedex 07, France, and Université Claude Bernard Lyon I, 43, Boulevard du 11 novembre 1918, 69622 Villeurbanne Cedex, France

Received October 21, 1998

We here present a quantum chemical analysis of the possible Peierls distortions accompanying charge redistribution in the $Pt_2(dta)_4I$ infinite chain. Starting with the building block calculations, we point out the participation of the $CH_3CS_2^-$ (dta) ligand in the mechanism of electron transfer. As the chain grows, the position and the geometry of the equatorial dta ligands are significantly altered. These changes indirectly control the Pt−I distances and lead to noticeable reduction of electron−phonon coupling through bridging halogen. These results agree with experimental data suggesting the involvement of internal degrees of freedom in the electron trapping phenomenon.

I. Introduction

Halogen-bridged transition-metal linear-chain compounds have attracted much interest due to their intriguing optical, magnetic and electrical properties.[1−4] The ground states of these one-dimensional (1D) systems strongly depend on the nature of the metal, the halogen, and the equatorial ligand(s) and, when included in the crystal structure, on the counterion. One can distinguish two major categories depending on the metal−halogen alternation. The first one contains compounds usually referred to as MX chains (M = Ni, Pd, Pt and X = Cl, Br, I), since halogen atoms separate mononuclear metallic complexes. This class of compounds has been studied extensively from both the experimental and theoretical aspects. One important example of such chain complexes is Wolfram's red salt (WRS), $[Pt^{II}(C_2H_5NH_2)_4][Pt^{IV}(C_2H_5NH_2)_4Cl_2]\cdot 4H_2O$. The peculiar point is that bridging halogen ions are displaced from midpoint positions, resulting in a charge density wave (CDW) characterized by alternating Pt^{II} and Pt^{IV} ions. The electronic and vibrational spectral properties related to this charge disproportionation are well documented.[1−4] On the basis of numerous model Hamiltonians[5−12] and quantum chemical treatments,[13−15] it was shown that strong electron−phonon interactions were responsible for the observed mixed-valence state in a series of WRS-type complexes. Several semiempirical calculations[13,15] agreed with the Peierls theorem which states that, for a strictly 1D system, the equidistant nuclear configuration of solids with partially filled energy bands is unstable with respect to a static deformation doubling the elementary cell. However, the nature of the ground state is governed by the competition between the electron−phonon interaction and the electronic correlation. Indeed, the latter might be strong enough, for instance, in Ni compounds, to occasionally give rise to a Ni^{III} Mott−Hubbard state.

More recently, an emerging class of new compounds known as MMX chains has attracted considerable attention.[16−30] The alternation of metallic dimers with a direct metal−metal bond

* To whom correspondence should be addressed. E-mail: borchtch@catalyse.univ-lyon1.fr.

† Institut de Recherches sur la Catalyse and Ecole Normale Supérieure de Lyon.

‡ Université Claude Bernard Lyon I.

(1) Day, P. In *Low-Dimensional Cooperative Phenomena*; Keller, H. J., Ed.; Plenum: New York, 1974; p 191.
(2) Keller, H. J. In *Extended Linear Chain Compounds*; Miller, J. S., Ed.; Plenum: New York, 1982; Vol. 1, p 357.
(3) Clark, R. J. H. In *Mixed Valency Systems: Applications in Chemistry, Physics and Biology*; Prassides, K., Ed.; Kluwer: Dordrecht, 1991; p 273.
(4) See, for example, corresponding chapters in the proceedings of the International Conferences on Synthetic Metals: *Synth. Met.* **1991**, *41*−*43*; **1993**, *55*−*57*; **1995**, *70*; **1997**, *86*.
(5) Tinka Gammel, J.; Saxena, A.; Batistic, I.; Bishop, A. R.; Phillpot, S. R. *Phys. Rev. B* **1992**, *45*, 6408.
(6) Nasu, K. *J. Phys. Soc. Jpn.* **1983**, *52*, 3865; **1984**, *53*, 302, 427.
(7) Baeriswyl, D.; Bishop, A. R. *J. Phys. C: Solid State Phys.* **1988**, *21*, 339.
(8) Huang, Q. F.; Wu, C. Q.; Sun, X. *Phys. Rev. B* **1995**, *52*, 5637.
(9) Mishima, A.; Nasu, K. *Phys. Rev. B* **1989**, *39*, 5758, 5763; **1989**, *40*, 5593.
(10) Wang, C. L.; Wang, W. Z.; Gu, G. L.; Su, Z. B.; Yu, L. *Phys. Rev. B* **1993**, *48*, 10788.
(11) Tagawa, Y.; Suzuki, N. *J. Phys. Soc. Jpn.* **1995**, *64*, 1800, 2212.
(12) Takeda, J.; Okada, M.; Kurita, S.; Tanaka, K.; Suemoto, T. *Phys. Rev. B* **1995**, *52*, 14441.
(13) Whangbo, M.-H.; Foshee, M. J. *Inorg. Chem.* **1981**, *20*, 113.
(14) Alouani, M.; Albers, R. C.; Wills, J. M.; Springborg, M. *Phys. Rev. Lett.* **1992**, *69*, 3104. Alouani, M.; Wilkins, J. W.; Albers, R. C.; Wills, J. M. *Phys. Rev. Lett.* **1993**, *71*, 1415.
(15) Robert, V.; Borshch, S. A.; Bigot, B. *Inorg. Chem.* **1996**, *35*, 3913.
(16) Che, C.-M.; Herbstain, F. H.; Snaefer, W. P.; Marsh, R. E.; Gray, H. B. *J. Am. Chem. Soc.* **1983**, *105*, 4604.
(17) Butler, L. G.; Zietlow, M. H.; Che, C.-M.; Schaefer, W. P.; Sridhar, S.; Grunthaner, P. J.; Swanson, B. I.; Clark, R. J. H.; Gray, H. B. *J. Am. Chem. Soc.* **1988**, *110*, 1155.
(18) Kurmoo, M.; Clark, R. J. H. *Inorg. Chem.* **1985**, *24*, 4420.
(19) Kimura, N.; Ohki, H.; Ikeda, R.; Yamashita, M. *Chem. Phys. Lett.* **1994**, *220*, 40.
(20) Yamashita, M.; Toriumi, K. *Inorg. Chim. Acta* **1990**, *178*, 140.
(21) Mitani, T.; Wada, Y.; Yamashita, M.; Toriumi, K.; Kobayashi, A.; Kobayashi, H. *Synth. Met.* **1994**, *64*, 291.
(22) Wada, Y.; Furuta, T.; Yamashita., M.; Toriumi, K. *Synth. Met.* **1995**, *70*, 1195.
(23) Bellito, C.; Flamini, A.; Gastaldi, L.; Scaramuzza, L. *Inorg. Chem.* **1983**, *22*, 444.
(24) Bellito, C.; Dessy, G.; Fares, U. *Inorg. Chem.* **1985**, *24*, 2815.
(25) Yamashita, M.; Wada, Y.; Toriumi, K.; Mitani, T. *Mol. Cryst. Liq. Cryst.* **1992**, *216*, 207.

10.1021/ic9812353 CCC: $18.00
Published on Web 03/12/1999

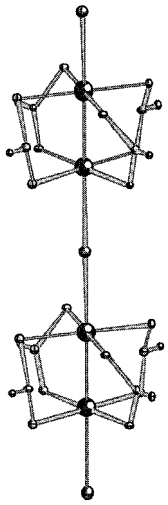

Figure 1. Schematic representation of MMX chains. The equatorial part is given by four dta ligands.

and halogen ions shapes the backbone of MMX compounds and is shown in Figure 1. The coordination sphere of metals is completed by four μ-bridging ligands L (L = $CH_3CS_2^-$ (dta),[23−29] $EtCS_2^-$ (dtp),[30a] *n*-$PrCS_2^-$ (dtbu),[30a] or $P_2O_5H_2^{2-}$ (pop)[16−22]), leading to the common stoichiometry $(M_2(L)_4X)^{n-}$.

Several representatives were synthesized and characterized by different techniques. The counterions influence the chain parameters, participate in hydrogen bonding, and contribute to steric effects. This sets two main families among MMX chains, namely, the "pop" and the "dta" chains. Unlike the pop compounds, the chains with dta, dtp, and dtbu ligands are neutral, giving rise to short-range interactions and quasi-1D species. Since the formal oxidation state of the transition metal is +2.5, MMX chains may exhibit different types of ordered valence structures.[28,29] The results obtained for the $Pt_2(dta)_4I$ chain from different experimental techniques are often contradictory. Several X-ray studies agree on equal Pt−I distances within the standard deviation (2.975 and 2.981 Å).[23,28,29] At the same time, on the basis of XPS[28,29] and Mössbauer[30b] spectral conclusions, it is now assumed that the low-temperature phase consists of halogen-bridged head-to-head dipoles $Pt^{II}-Pt^{III}$ (...−$Pt^{II}Pt^{III}$−I−$Pt^{III}Pt^{II}$−I−$Pt^{II}Pt^{III}$...). Here we address the crucial issue of the mechanism involved in this Peierls transition. In disagreement with experimental data, Whangbo and Canadell previously predicted within the extended Hückel band framework a Peierls-type distortion through displacements of bridging halogens.[31] More recently we have investigated the role of different types of distortions in MMX chains on the basis of two comparative approaches.[32] Interactions with two types of ligand vibrations (internal and external) were effectively taken into account in the phenomenological vibronic model. We showed that an infinite chain could undergo Peierls transition through external and/or internal modes. Strong intradimer electron-vibrational interaction resulting from the twisting distortion of dta ligand was suggested as a possible driving force in the Peierls transition. Semiempirical band calculations as well as a phenomenological model of vibronic origin supported the valence distribution ...−$Pt^{II}Pt^{III}$−I−$Pt^{III}Pt^{II}$−.... Besides, tight-binding optimizations did not display any displacement of bridging halogen from the symmetric position, in agreement with the X-ray data for the $Pt_2(dta)_4I$ chain. Among other 1D systems in which along-chain electron transfer is governed by twisting of equatorial ligands one should mention the tetracyanoplatinate[33] and NiPcI (Pc = phthalocyanine)[34] chains.

The experimental data that had long given rise to much controversy have apparently led to theoretical disagreement on the origin of Peierls distortion in MMX chains. Therefore, we analyzed the mechanism for charge redistribution in a platinum chain. Our goal was first to give some new insights into the participation of internal (i.e., twisting distortion of dta ligand) and external (i.e., stretching distortion of Pt−I bonds) degrees of freedom and their interdependence in the Peierls transition. To clarify the local origin of charge transfer in the $Pt_2(dta)_4I$ chain, we also studied two hypothetical building blocks. Since Peierls distortion is accompanied by an enlargement of the unit cell, these clusters were chosen to reproduce the motif $[Pt_2(dta)_4I]$ and the dimerized motif $[Pt_4(dta)_8I]$. The Pt coordination spheres were completed by one and two iodine atoms for the dimer and the tetramer, respectively. It gives rise to two clusters $[Pt_2(dta)_4I_2]$ and $[Pt_4(dta)_8I_3]$. In this way, we were able to draw conclusions on the relative participation of local and collective effects in the charge redistribution process. Our recent study[15] of some MX chains suggested that disproportionation can already occur in the elementary "bricks" of the infinite chain. Also, the analysis of small fragments allows the evaluation of the interdependence of different types of distortions which can occur in the infinite chain. Cluster models are known to be a reliable tool to study 1D charge-transfer systems.[35−37]

In the next section, the methodology we developed and quantum chemical tools we used are briefly summarized. In section III, we consider hypothetical dimeric (section III.A) and tetrameric (section III.B) building blocks to get an understanding of the local equilibrium geometries and valence pattern. We performed ab initio calculations for several oxidation states of platinum atoms, namely, +2, +2.5, and +3, and carried out an orbital analysis of the trend in the metal−halogen distances. In section IV, a semiempirical tight-binding scheme was used to elucidate some of the characteristic properties of mixed-valence chain compounds. The stability of the homogeneous chain with formal oxidation state +2.5 is studied with respect to several electron trapping distortions.

II. Methodology

Since we were mainly interested in looking into the different mechanisms involving charge transfer, we decided to first focus on the simplest dimeric unit reported as the starting material for platinum chain synthesis, namely, $[Pt_2(dta)_4I_2]$ (Figure 2a). On the basis of ab

(26) Shirotani, I.; Kawamura, A.; Yamashita, M.; Toriumi, K.; Kawamura, H.; Yagi, T. *Synth. Met.* **1994**, *64*, 265.
(27) Ikeda, R.; Kimura, N.; Ohki, H.; Furuta, T.; Yamashita, M. *Synth. Met.* **1995**, *71*, 1907.
(28) Kitagawa, H.; Onodera, N.; Ahn, J.-S.; Mitani, K.; Misa, K.; Ozawa, Y.; Toriumi, K.; Yasui, K.; Manabe, T.; Yamashita, M. *Mol. Cryst. Liq. Cryst.* **1996**, *285*, 311.
(29) Kitagawa, H.; Onodera, N.; Ahn, J.-S.; Mitani, K.; Toriumi, K.; Yamashita, M. *Synth. Met.* **1997**, *86*, 1931.
(30) (a) Mitsumi, M.; Murase, T.; Matsumoto, M.; Ozawa, Y.; Toriumi, K.; Kobayashi, M.; Sonoyama, T.; Kitagawa, H.; Mitani, T. In *Book of Abstracts*, XXXIII International Conference on Coordination Chemistry; CNR: Florence, 1998; p 385. (b) Kitagawa, H.; Sonoyama, T.; Yamamoto, M.; Mitani, T.; Toriumi, K.; Yamashita, M. *Idem*, p 84.
(31) Whangbo, M.-H.; Canadell, E. *Inorg. Chem.* **1986**, *25*, 1727.
(32) Borshch, S. A.; Prassides, K.; Robert, V.; Solonenko, A. O. *J. Chem. Phys.* **1998**, *109*, 4562.
(33) Whangbo, M.-H.; Hoffmann, R. *J. Am. Chem. Soc.* **1978**, *100*, 6093.
(34) Mikkelsen, K. V.; Ratner, M. A. *Chem. Rev.* **1987**, *87*, 113 and references therein.
(35) Prassides, K.; Schatz, P. N.; Wong, K. Y.; Day, P. *J. Phys. Chem.* **1986**, *90*, 5588.
(36) Prassides, K.; Schatz, P. N. *J. Phys. Chem.* **1989**, *93*, 83; *Chem. Phys. Lett.* **1991**, *178*, 227.
(37) Painelli, A.; Girlando, A. *J. Chem. Phys.* **1986**, *84*, 5655.

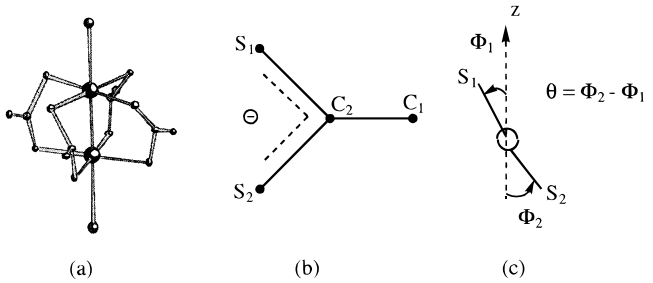

Figure 2. (a) Dimer unit used in our cluster calculations ($Pt_2(dta)_4I_2$ or $Pt_2(dta)_4Br_2$). (b) Schematic representation of the dta ligand. (c) Newman projection showing the tilting ($\theta = 0$) and twisting ($\theta \neq 0$) distortions of the dta ligand. The ϕ angles are given in order of occurrence along the chain.

Table 1. Optimized and Experimental Values for $Pt_2(dta)_4Br_2$ Geometrical Parameters

bond distances and angles	exptl[a]	calcd[b]
Pt−Pt (Å)	2.57	2.61
Pt−Br (Å)	2.57	2.65
Pt−S (Å)	2.38	2.44
Pt−S−C (deg)	106.8−109.3	108.6
S−Pt−S (deg)	86.6−91.5	90.1

[a] From ref 38. [b] RHF calculations.

initio calculations, we traced the magnitude of stretching symmetrical distortions with regard to the infinite chain in the following species, $[Pt_2(dta)_4I_2]$ and $[Pt_4(dta)_8I_3]$. The next step was to clarify the role of the dta ligand twisting mode (Figure 2c) in electron transfer by means of the low-time-consuming extended Hückel approach. For this type of distortion semiempirical methods are known to give quite realistic results.

Unfortunately, no crystallographic data were available for the isolated compound where the two platinum atoms are in oxidation state +3. However, the crystal structure of parent dimer compound $[Pt_2(dta)_4Br_2]$ has been recently resolved[38] and comparisons between experimental data and our calculations were drawn to assess the level of accuracy. On the basis of an ab initio restricted-Hartree−Fock (RHF) approach implemented in the Gaussian94 (G94) package,[39] the optimized parameters for this closed-shell bromine compound turned out to be in rather good agreement with experimental X-ray data (Table 1).

The second technical issue we addressed was the contribution of correlation effects in the optimized structure. By means of the hybrid method B3LYP based on DFT and available in the G94 package, we again optimized the geometry of the $[Pt_2(dta)_4Br_2]$ dimer. No significant deviations from RHF calculations were observed (less than 3%), a reflection of weak correlation in platinum species. Since relevant and conclusive comparisons were made from the results obtained on our probe molecule $[Pt_2(dta)_4Br_2]$, all optimizations were performed within RHF and B3LYP approaches for closed-shell and open-shell systems, respectively. Throughout these calculations the LanL2DZ basis set[39] was used.

In addition, extended Hückel calculations were used not only to qualitatively estimate the twisting angle values but also to provide molecular orbital analysis. Such a semiempirical approach was found to be quite reliable for the study of the stabilities of these centrosymmetric structures. The diagonal matrix elements and orbital exponents used in the extended Hückel theory are presented in Table 2. A modified Wolfsberg−Helmoltz formula was used to calculate off-diagonal matrix elements.

(38) Toriumi, K.; Yamashita, M. Unpublished results.
(39) Frisch, M. J.; Trucks, G. W.; Schlegel, H. B.; Gill, P. M. W.; Johnson, B. G.; Robb, M. A.; Cheeseman, J. R.; Keith, T.; Petersson, G. A.; Montgomery, J. A.; Raghavachari, K.; Al-Laham, M. A.; Zakrzewski, V. G.; Ortiz, J. V.; Foresman, J. B.; Peng, C. Y.; Ayala, P. Y.; Chen, W.; Wong, M. W.; Andres, J. L.; Replogle, E. S.; Gomperts, R.; Martin, R. L.; Fox, D. J.; Binkley, J. S.; DeFrees, D. J.; Baker, J.; Stewart, J. J. P.; Head-Gordon, M.; Gonzales, C.; Pople, J. A. *Gaussian 94*; Gaussian, Inc.: Pittsburgh, PA, 1995.

Table 2. Atomic Parameters[a]

μ	ζ_μ	ζ_ν	$H_{\mu\mu}$ (eV)
Pt 6s	2.554		−9.08
Pt 6p	2.554		−5.48
Pt 5d[b]	6.013 (0.6333)	2.696 (0.5512)	−11.26
I 5s	2.679		−18.0
I 5p	2.322		−12.7
S 3s	2.122		−20.0
S 3p	1.827		−11.0
C 2s	1.625		−21.40
C 2p	1.625		−11.40
H 1s	1.300		−13.60

[a] The d orbitals are given as linear combinations of two Slater-type functions, and each is followed in parentheses by the weighting coefficient. [b] Reference 40.

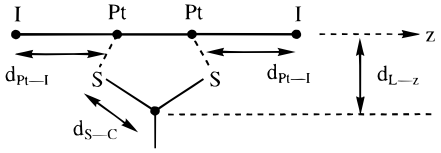

Figure 3. Representation of the dimer unit backbone with ab initio optimized parameters.

Table 3. Optimized Distances for d^7-d^7 and d^7-d^8 Electronic Configurations

distance (Å)	d^7-d^7	d^7-d^8	$Pt_2(dta)_4I$ chain
d_{Pt-I}	2.87	3.06	2.98
d_{L-z}	3.16	3.16	3.02

III. Vibronic Interactions in the Hypothetical Building Blocks

III.A. Dimer Unit $[Pt_2(dta)_4I_2]^{n-}$. Two different electronic configurations were considered, namely, d^7-d^7 (i.e., $[Pt_2(dta)_4I_2]$) and d^7-d^8 (i.e., $[Pt_2(dta)_4I_2]^-$), which correspond to formal Pt oxidation states +3 and +2.5, respectively. The former configuration is found in the starting material, whereas the latter is expected to be present in the polymeric system. The parameters used in the ab initio optimizations are defined in Figure 3. It should be emphasized that the two platinum atoms remain strictly equivalent in the calculations and that the planar resonant structure (see Figure 2b) of the four dta ligands is preserved. The important result is that the dta ligands move away from the iodine−platinum backbone (z axis in Figure 3) compared to their reported equilibrium positions in the chain (Table 3). As a matter fact, the dta distance to the z axis (d_{L-z} in Figure 3) increases by 0.14 Å. Since d_{L-z} is essentially independent of electron configuration, one may assume that the increase in d_{L-z} results mainly from the absence of the steric interchain interactions. By contrast, as can be seen from Table 3 the Pt−I distance d_{Pt-I} is very sensitive to oxidation state. First, d_{Pt-I} increases upon reduction as one would expect from simple electrostatic considerations.

A convincing picture for these distance changes between the chain and the isolated dimers can be obtained from a fragment molecular orbital approach (FMO) (Figure 4). As d_{L-z} increases, $d_{z^2}^*$ the antibonding orbital of the $[Pt_2(dta)_4]$ fragment is lowered. The interaction with the symmetry-adapted orbital of the $[I_2]$ fragment, namely, the antibonding orbital, is therefore enhanced (Figure 4a). For the d^7-d^7 configuration, $d_{z^2}^*$ is the LUMO. The resulting 2-electron interaction is more effective when the iodine ions move toward the platinum atoms. Conversely, a 3-electron interaction is dominant in the d^7-d^8 configuration: d_{Pt-I} increases to reduce the disfavorable splitting (Figure 4b). Thus, the distance ordering observed in our ab initio

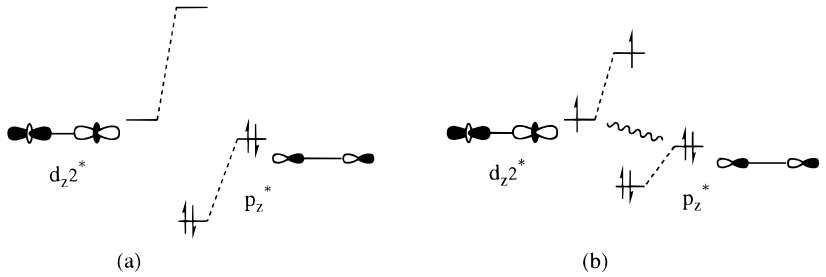

Figure 4. Molecular orbital diagram. The main contributions to each valence orbital are shown. (a) 2-Electron interaction resulting in a net reduction of the Pt−I distance. (b) 3-Electron interaction pushing the two iodine ions away.

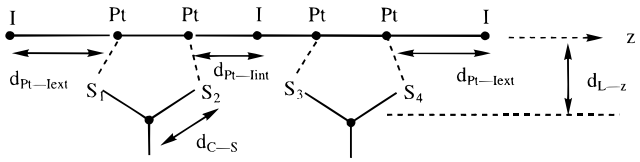

Figure 5. Representation of the tetramer unit backbone with ab initio optimized parameters.

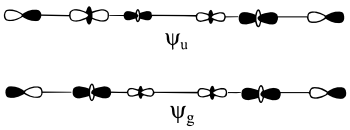

Figure 6. Valence orbitals of the $[Pt_4(dta)_8I_3]^-$ compound. ψ_g is the HOMO, ψ_u the LUMO.

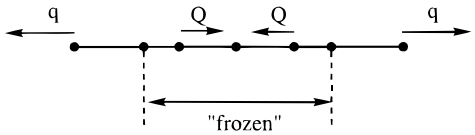

Figure 7. Relaxation accompanying the 2-electron reduction of the $[Pt_4(dta)_8I_3]^+$ compound.

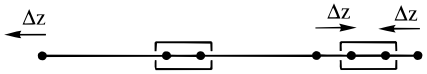

Figure 8. Breathing distortion leading to the pseudo-Jahn−Teller stabilization of $[Pt_4(dta)_8I_3]^-$.

calculations is well-understood in this FMO analysis and supports the important role of the dta ligand in determining the strength of the electronic interaction along the *z* direction.

The next step was to trace the influence of angular distortions parametrized by ϕ_1 and ϕ_2 (see Figure 2c). These parameters describe a staggered conformation of [S4] planes around the Pt atoms without loss of planarity of the dta ligand as long as $\phi_1 = \phi_2$. Whenever $\phi_1 \neq \phi_2$ (twisting distortion), the equivalence between the two platinum atoms is disrupted, leading to the electron localization on one part of the cluster. At this point, extended Hückel calculations were performed since they are known to give qualitatively satisfactory results. The optimum geometry for the two electronic configurations was found for $\phi_1 = \phi_2 \approx 20°$. The staggered conformation of [S4] squares in the chain is characterized by a 21° angle.[23] No significant twisting distortion was observed, and since the planarity of the dta ligand is not altered, the π-system remains delocalized. Within the framework of our description, the $[Pt_2(dta)_4I_2]^-$ model dimer belongs to class III in the Robin and Day classification.

III.B. Tetramer Unit $[Pt_4(dta)_8I_3]^{\pm}$. In the solid state, the Peierls distortion is known to formally increase the unit cell. To fill out the framework of our approach, we chose to investigate the hypothetical clusters $[Pt_4(dta)_8I_3]^{\pm}$ reflecting the dimerized unit cell of the infinite chain (Figure 5). $[Pt_4(dta)_8I_3]^+$ and $[Pt_4(dta)_8I_3]^-$ correspond to $d^7-d^7-d^7-d^7$ and $d^7-d^7-d^8-d^8$ closed-shell electronic configurations, respectively.

Our goal was to obtain insight on the nature of the structural changes of the 4-Pt^{III} system ($d^7-d^7-d^7-d^7$ configuration) occurring upon 2-electron reduction. Following the methodology described in section III.A, we first optimized a set of parameters (see Figure 5) for the two oxidation states on the basis of ab initio RHF calculations. The two d_{L-z} values were found to be equal to 3.14 Å and slightly differ from the distances in the dimer. To begin with, we allowed for the four Pt−I distances two degrees of freedom, $d_{Pt-I_{int}}$ and $d_{Pt-I_{ext}}$ shown in Figure 5. If one considers the $d^7-d^7-d^7-d^7$ LUMO (ψ_g in Figure 6), a 2-electron reduction should lead to the lengthening of all Pt−I bonds. As seen from Table 4, the predicted trend is not observed whereas the distance between the terminal Pt atoms is essentially not sensitive to oxidation state (≈11.4 Å). Therefore the observed relaxation retains inversion symmetry and can be parametrized by the gerade mode {*q*, *Q*} in Figure 7.

Table 4. Optimized Distances for $d^7-d^7-d^7-d^7$and $d^7-d^7-d^8-d^8$ Electronic Configurations

distance (Å)	$d^7-d^7-d^7-d^7$	$d^7-d^7-d^8-d^8$
$d_{Pt-I_{int}}$	3.09	2.92
$d_{Pt-I_{ext}}$	2.73	3.14

Let us focus on the changes in the structure and the energy of orbital ψ_g arising by filling this orbital with two electrons. An equilibrium description of the geometrical and electronic structure can be found by tracing the energy of the system as a function of {*q*, *Q*}. This procedure yields maximum stabilization enegy of 0.60 eV at $q = 0.40$ Å and $Q = 0.20$ Å. The equilibrium structure is a compromise between two dominant phenomena: on one hand, the reduction of a strong antibonding interaction of terminal iodine ions with the metals, and on the other hand, a growth of bonding character between Pt−Pt units. Mulliken charge analysis indicates formal $[Pt^{IV}Pt^{II}-Pt^{II}Pt^{IV}]^+$ and $[Pt^{II}Pt^{III}-Pt^{III}Pt^{II}]^-$ valence distributions, in agreement with a purely ionic Pt−I bond length description. We then studied the stability of these symmetrical structures against two types of distortions, the "breathing" stretching mode (Figure 8) and angular deformations of the dta ligand (see Figure 2c). None of the two clusters examined is significantly prone to symmetry breaking by angular deformation. Indeed, the equilibrium geometry was found at $\phi_1 = \phi_2 = \phi_3 = \phi_4 \approx 18°$.

In contrast, the potential surface is sensitive to iodine displacement and oxidation state. Unlike the oxidized cluster $[Pt_4(dta)_8I_3]^+$, the equilibrium geometry for $[Pt_4(dta)_8I_3]^-$ was found to be asymmetric due to displacement $\Delta z = 0.20$ Å. This result is in good agreement with the conclusions of orbital models as the population of high-lying levels favors the asymmetric geometry with increasing effective vibronic con-

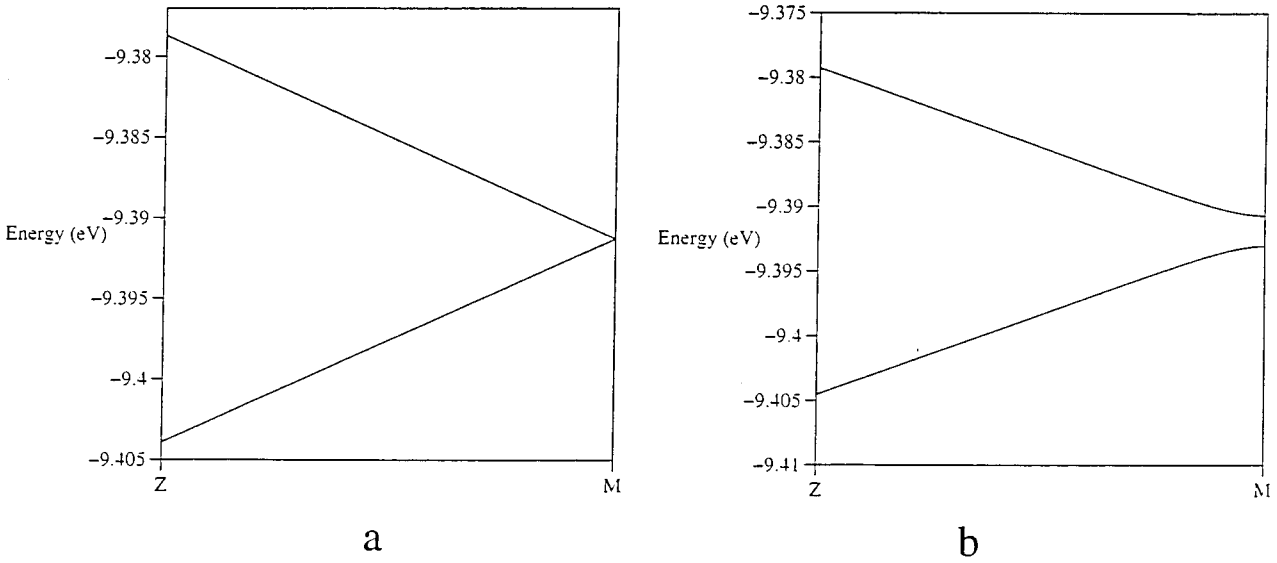

Figure 9. Band dispersion curves in the vicinity of the Brillouin zone edge (Z(0.49) and M(0.5) in reciprocal space vector units $2\pi/a$): (a) $\phi_1 = \phi_2 = \phi_3 = \phi_4 \approx 12°$; (b) $\phi_1 = \phi_4 = 9°$, $\phi_2 = \phi_3 = 14°$.

stant.[41] If one focuses on the quasi-degenerate highest occupied orbitals ψ_u and ψ_g of $[Pt_4(dta)_8I_3]^-$, strong electron-vibrational interaction with the "ungerade" breathing mode is expected through a nonzero matrix element. The estimated 0.14 eV pseudo-Jahn−Teller stabilization energy is mainly responsible for the favorable interaction with the off-center bridging halogen. Upon distortion, the charge distribution evolves from $[Pt^{II}Pt^{III}-Pt^{III}Pt^{II}]^-$ to $[Pt^{II}Pt^{II}-Pt^{III}Pt^{III}]^-$, reflecting interdimer electron transfer. No contribution of the dta ligands in "ungerade" distortions was found.

These results strongly suggest that the dta ligand actually participates in charge redistribution through a modulation of the interactions between platinum and iodine atoms. The Pt−I stretching mode is very sensitive to the equilibrium position of dta. Thus, the computational results for the tetramers (i.e., "breathing" relaxation) point toward the indirect control of the longitudinal electron transfer by the equatorial ligands. The charge disproportionation observed in the doubled elementary cell results from halogen antisymmetric displacements with negligibly small participation of the dta ligand twisting distortion.

IV. Vibronic Interactions in the $Pt_2(dta)_4I$ Chain

Experimental studies and previous theoretical calculations showed that the twisting of the dta ligand could account for the Peierls distortion in $Pt_2(dta)_4I$.[28,29,32] One major piece of evidence reflecting the role of this distortion is the structural phase transition in the temperature range 255−375 K, resulting from the disorder in the helical structure of Pt dimers.[28,29] These structural changes are accompanied by a semiconductor−metal transition. In our previous theoretical approach,[32] the dta ligand geometry was optimized for different twisting-angle values through ab initio SCF-type calculations. We showed that the valence structure $Pt^{II}Pt^{III}-I-Pt^{III}Pt^{II}$ results from the anti-phase ordering of twisting distortions in neighboring dimers. However, only a limited number of molecular orbitals and nearest neighbor interactions (i.e., S−Pt) were taken into account in the semiempirical band calculations. We therefore tried to elucidate the actual participation of the chelating dta ligand including those distortional modes which were ignored in previous semiempirical calculations.[31] The role of bridging iodine in the process of charge redistribution was traced as well. Thus, within extended Hückel band calculations implemented in the YAeHMOP program,[42] the stability of a homogeneous Pt(+2.5) 1D chain was investigated with respect to different dimerizing deformations. A doubled unit cell consisting of two dimer units was used to allow flexibility in the number of degrees of freedom involved. First, we studied the chain stability against angular deformation of the dta ligands. As for the hypothetical tetramer unit, we noticed a significant stabilization with the nontrapping distortion parametrized by $\phi_{min} = \phi_1 = \phi_2 = \phi_3 = \phi_4 \approx 12°$ (see Figure 2c). However, the disruption of the dta π-delocalized system is a nonactivated process (less than 0.01 eV) characterized by $\phi_1 = \phi_4 = 9°$ and $\phi_2 = \phi_3 = 14°$ and results in a valence distribution $Pt^{II}Pt^{III}-I-Pt^{III}Pt^{II}$ evidenced in previous studies.[32] The dependence of the highest occupied band, namely the $d^*_{z^2}$ band, upon twisting parameter $\theta = \phi_1 - \phi_2 = \phi_4 - \phi_3$ is given in Figure 9. One should point out the degeneracy splitting, a reflection of Peierls distortion. The relative softness of the adiabatic potential accounts for the system ability to undergo phase transition even at low temperature. However, a Peierls-type halogen displacement was also found when further optimization was performed. Its value (0.16 Å) is less important than in the hypothetical tetramer (see section III.B). Therefore one can suggest that, along with the chain lengthening, three correlated phenomena occur: (i) the tilt of the dta ligand parametrized by the ϕ angle is reduced; (ii) the magnitude of the dta twisting distortion is enhanced; (iii) the off-center halogen displacement decreases. These observations again underline how significantly the dta ligand is involved in the mechanism of valence structure shaping.

V. Conclusion

Our analysis shows that the electronic structure of the $Pt_2(dta)_4I$ chain is determined by the intimate competition between different factors. Our analysis of the elementary blocks shows that the particularity of the $Pt_4(dta)_4I$ chain may lie in the effective participation of the equatorial ligand. Both the relative

(40) Bigot, B.; Delbecq, F.; Peuch, V.-H. *Langmuir* **1995**, *11*, 3828.
(41) Robert, V. Ph.D. Thesis, Ecole Normale Supérieure de Lyon, Lyon, 1996.
(42) Landrum, G. A. YAeHMOP: Yet Another extended Hückel Molecular Orbital Package.

position of the dta ligand with respect to the chain axis (distance and tilting angle) and the twisting distortion govern the charge redistribution. The Peierls-type band gap opening can occur not only through bridging halogen displacements as it was previously shown by Whangbo and Canadell[31] but also through the internal twisting of the dta ligand. In the real system only the latter is observed. Even though full agreement with the experiment is not reached, we found that the dta distortion reduces the amplitude of the iodine displacement, i.e., effective electron−phonon coupling for interdimer vibrations. Considering the building block analysis, the collective effects seem to play a decisive role in the electron trapping phenomenon. Further, more accurate electronic structure calculations for the infinite system are certainly needed and should give special consideration to a detailed description of the dta ligand. Alternatively, some new interactions which could favor one particular type of distortion should be taken into account. For example, interchain contacts through dta ligands will certainly modify the equilibrium structural parameters in the real 3D solid.

Acknowledgment. The authors thank H. Kitagawa, K. Toriumi, and M. Yamashita for fruitful discussion and for providing us with the structural data of the $Pt_2(dta)_4Br_2$ compound prior to publication.

IC9812353